SiliconPV 2024, 14th International Conference on Crystalline Silicon Photovoltaics
Silicon Material and Defect Engineering
https://doi.org/10.52825/siliconpv.v2i.1336

Published: 06 Dec. 2024

Implied J-V Curves Recorded at Elevated Temperatures Using Light Controlled Heating

Gergely Havasi[1,2], Dávid Krisztián[1,2], Ferenc Korsós[1], and Shaoyong Fu[3]

[1] Semilab Co. Ltd., Hungary

[2] Department of Physics, Institute of Physics, Budapest University of Technology and Economics, Hungary

[3] Semilab Trade Shanghai Co., Ltd., China

*Correspondence: Gergely Havasi, gergely.havasi@semilab.hu

Abstract. The carrier lifetime characterization of solar cells is typically performed at room temperature, although the operational temperature of a solar panels can reach 60 °C. We realized a setup for laser controlled photoconductance decay (PCD) measurement at elevated temperatures induced by light. We investigated precursor p-PERC cells from multiple parts of the same ingot using this technique. From the injection level dependent carrier lifetime results the implied current-voltage characteristics are evaluated as well. We observed a relatively small but noticeable increase of the carrier lifetime up to 30% with increasing the temperature from 30°C to 60°C in all samples. Saturation current values obtained using the Kane-Swanson method indicate, that not only the bulk lifetime improves but the surface recombination rate weakens. Temperature coefficient values of the implied cell efficiency are around -0.35 rel%/°C and slightly below which agrees with typical results of electrical tests. However, due to the minor increase of the carrier lifetime, this is still a bit above the value one can obtain theoretically considering purely the known decrease of the open circuit voltage caused by the increased intrinsic charge carrier concentration at higher temperatures.

Keywords: Lifetime, Characterization, Implied J-V

1. Introduction

The electrical characterization of solar cells is typically performed at room temperature, although the operational temperature of a solar panels can reach 60 °C. There are only a few studies discussing it using contact I-V measurements of cells, but implied J-V (also known as pseudo J-V) results at elevated temperatures applying contactless photoconductance decay (PCD) techniques have not been demonstrated so far.

The character of the implied J-V characteristics from precursor cells is governed by the dependence of the recombination rate on the injection level Δn. The open-circuit nature of the PCD method enables to obtain the implied *J-V* curve in a contactless way [1], [2]. The implied open-circuit voltage Voc can be directly calculated at each Δn during the decay, as:

$$V_{oc}(\Delta n) = \frac{k_B T}{q} \ln \frac{\Delta n \, (\Delta n + N_{dop})}{n_i^2(T)}, \quad (1)$$

where k_B is the Boltzmann factor, T is the temperature, q is the charge of the electron, N_{dop} is the doping level, and n_i is the intrinsic charge carrier concentration. The recombination rate determines the diode current of the solar cell in the absence of electrical contacts.

$$J_{diode}(\Delta n) = -\frac{\partial \Delta n}{\partial t} qW, \tag{2}$$

where W is the thickness of the wafer. Then the implied $V_{oc}(\Delta n)$, and the

$$J(\Delta n) = J_{sc}(1sun) - J_{diode}(\Delta n) \tag{3}$$

functions can be interpreted as the terminal voltage and current values at 1 sun illumination level under different loads corresponding to a given Δn. This formula is applicable to calculate the implied J, since in the absence of physical contacts, there is no external current and so resistive losses do not appear either. Therefore, this implied J-V method characterizes purely the recombination related losses and defines an upper limit of the final cell performance.

Recombination losses in emitter region of the solar cell is commonly characterized by the emitter saturation current density J_0 determined from $\tau(\Delta n)$ using the Kane-Swanson method [3]. It relies on the hypothesis that forward bias current from the emitter layer is responsible for the shape of $\tau(\Delta n)$ at high Δn levels, if intrinsic recombination rates are compensated properly:

$$\frac{1}{\tau_{eff}(\Delta n)} - \frac{1}{\tau_{Auger}(\Delta n)} - \frac{1}{\tau_{rad}(\Delta n)} = \frac{1}{\tau_{SRH}} + \frac{J_0(N_{dop}+\Delta n)}{qWn_i^2}. \tag{4}$$

2. Measurement setup

The schematic drawing of the experimental setup is depicted in Fig. 1/a. The PCD measurement is realized using a 980 nm exciting laser and a calibrated radiofrequency eddy current sensor (RF antenna) below the wafer. The illumination spot was largened by homogenizing optics to generate homogeneous excess carrier distribution in the wafer around the sensed area of the RF antenna to avoid lateral carrier spreading effects.

The temperature of the wafer was measured using a calibrated in-situ infrared temperature sensor below the RF antenna. A high power 915 nm CW laser is responsible for the sample heating. The wafer was placed between two plexiglass sheets as “encapsulation” and therefore serving the thermal insulation of the wafer. Heating and PCD probing laser pulses are alternating periodically, as illustrated in Fig. 1/b inducing periodic carrier density waveforms (Fig. 1/c) to obtain the PCD decay curves. The variation of the wafer temperature during the PCD measurement was negligible (<0.05 °C) thanks to the insulating plexiglass sheets.

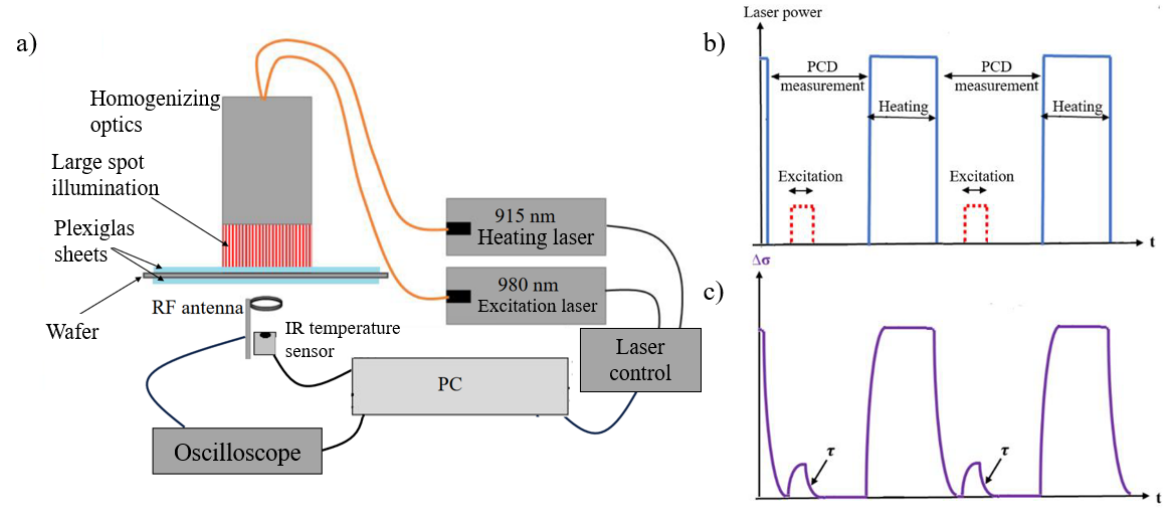

Figure 1. *Schematic illustration of the measurement setup (a), the PCD probing and heating laser pulses (b) and the induced excess carrier density Δn(t) (c).*

Since, the signals at low injection levels are noisy, we use a complex routine to smooth the recorded PCD decay curves which includes both a smart averaging and adaptive curve fitting procedure. An example of the PCD transient smoothing procedure is presented in Fig. 2. Fig. 2/a. depicts the locally averaged datapoints (as orange dots) used for later steps of the evaluation process, which is followed by fitting the calculated $\tau(\Delta n)$ curve using a suitable mathematical function, which is finally the reported result. Thes example shown in Fig. 2/b. illustrates the efficiency of this method comparing the $\tau(\Delta n)$ curves with and without these processes in the case of a severely noisy PCD transient.

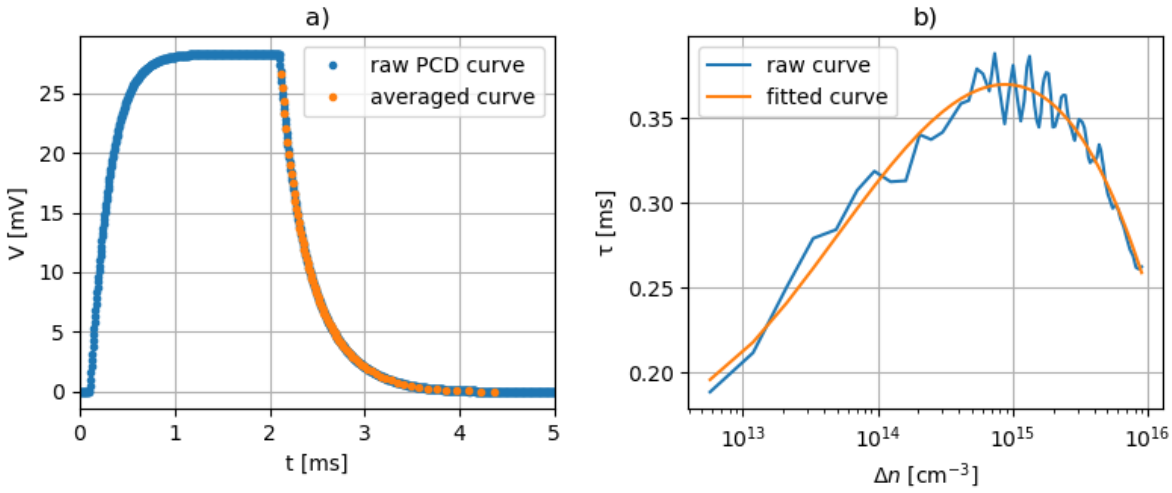

Figure 2. *Raw PCD measurement and the averaged points (a) and the $\tau(\Delta n)$ calculated from the averaged points and the fitted $\tau(\Delta n)$ curve (b).*

3. Results

Precursor wafers from a p-PERC production were tested using the method. Wafers are chosen from the same ingot pulled as the sixth ingot in a recharge Czochralski (RCz) sequence. Therefore, the wafers are expected to exhibit significant variation in contamination level, and therefore in bulk carrier lifetime.

One wafer was chosen from each of the top segment (with [Ga]=1.53·10^{16} cm^{-3} doping), middle segment ([Ga]=2.72·10^{16} cm^{-3}) and tail segment ([Ga]=3.50·10^{16} cm^{-3}). The investigated temperature range was from 30 °C to 60 °C. We used the Klaassen mobility model [4] to calculate the carrier concentration at different wafer temperatures from the measured sheet conductance. The Klaassen mobility model was also used to calculate the sheet resistance of the reference wafers for the calibration of the eddy-current sensor at different temperatures.

The measured $\tau(\Delta n)$ curves are depicted in Fig. 3/a. (wafer from ingot top), Fig. 4/a. (wafer from ingot middle) and Fig. 5/a. (wafer from ingot tail) at different temperatures. The injection level and lifetime values corresponding to the maximal power points (MPP) are marked with red dots. The recombination lifetime increases with the temperature, results in a reduced implied efficiency loss.

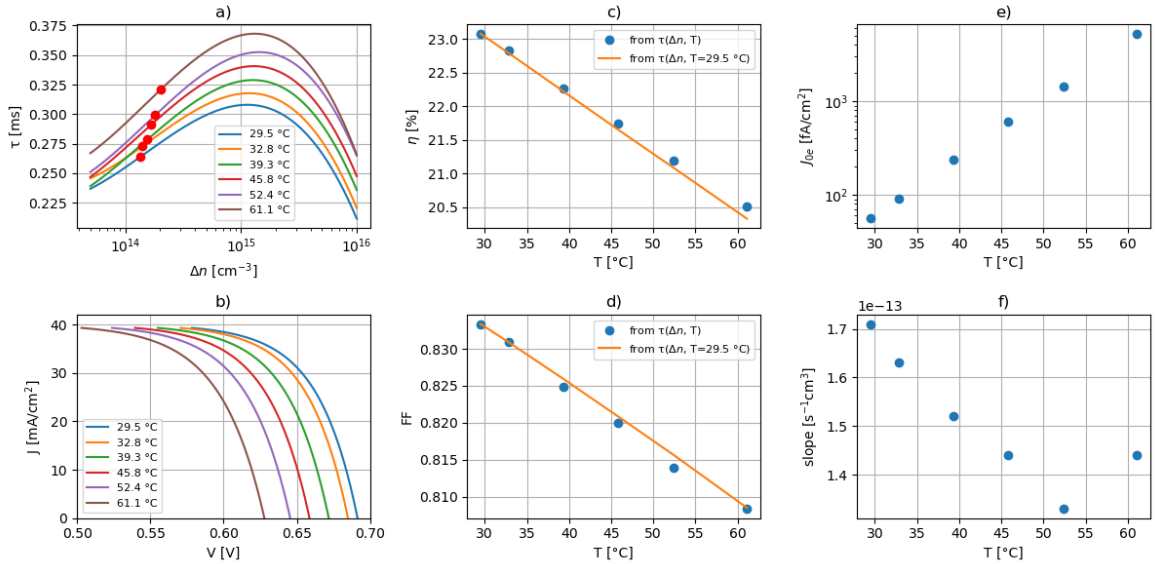

Figure 3. *Results related to the wafer from the top part of the ingot. τ(Δn) curves (a) and the calculated implied J-V curves (b) at different temperatures. The corresponding implied η(T) (c) and implied FF(T) (d). The recorded J_0(T) (e) and the slope of Kane-Swanson fit (f).*

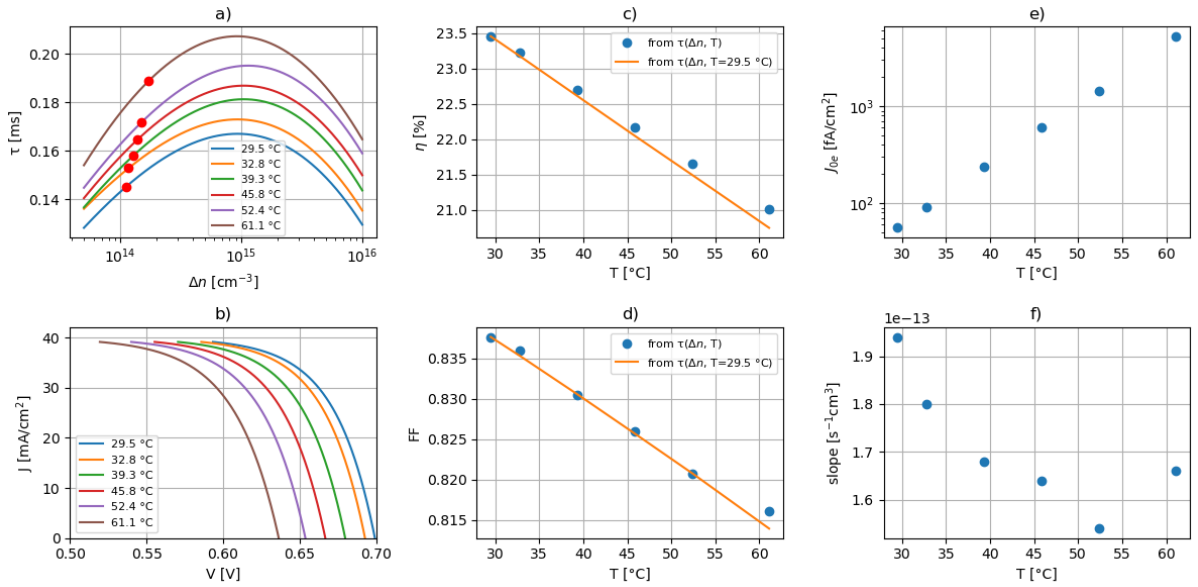

Figure 4. *Results related to the wafer from the middle part of the ingot. τ(Δn) curves (a) and the calculated implied J-V curves (b) at different temperatures. The corresponding implied η(T) (c) and implied FF(T) (d). The recorded J_0(T) (e) and the slope of Kane-Swanson fit (f).*

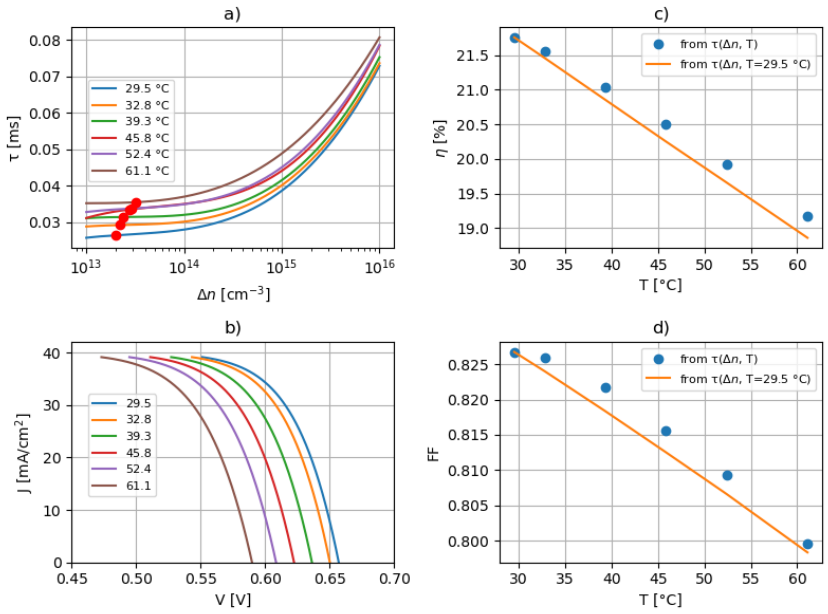

Figure 5. *Results related to the wafer from the tail part of the ingot. τ(Δn) curves (a) and the calculated implied J-V curves (b) at different temperatures. The corresponding implied η(T) (c) and implied FF(T) (d).*

The implied $V_{oc}(\Delta n)$, and the implied $J(\Delta \mathrm{n})$ functions were calculated using Eq. 1-2. and the implied *J-V* curves (Fig. 3/b., Fig. 4/b. and Fig. 5/b.) are depicted using $J_{sc}(1sun) = 40mA/cm^3$ as a typical data of PERC cells to convert the short circuit current to Suns unit. The Green model [5] was applied to determine $n_i(T)$ ignoring the band gap narrowing phenomenon at high Δn, but it was found to have negligible effect in this study.

The 1 sun equivalent implied *J-V* curve and determined implied cell parameters are plotted in Fig. 3/b-d. and Fig. 4/b-d. in the function of the temperature. One can observe, that the implied V_{oc} values are shifted due to the increased n_i at higher temperatures, while the implied current density values does not change significantly. The average, practically linear implied efficiency and implied FF drop was found to be -0.356 rel%/°C (top), -0.349 rel%/°C (middle) and -0.375 rel%/°C (tail), respectively. These values are close to results of contact measurements on final cells, which indicates the reliability of our method.

To separate the effect of the temperature dependence of $\tau(\Delta n)$ from the inevitable impact of $n_i(T)$, the measured implied efficiency $\eta(T)$ and implied fill factor FF(T) curves are compared to implied $\eta(T)$ and implied FF(T) considering only $n_i(T)$, so using $\tau(\Delta n)$ measured at 30°C to calculate them (orange lines in Fig. 3/c-d and Fig. 4/c-d). We found that the temperature dependency of $n_i(T)$ dominates the η drop. Carrier lifetimes increase in the function of temperature in the entire Δn range (Fig. 3/a, Fig. 4/a and Fig. 5/a) but increasing η only slightly. The improvement of carrier lifetime at elevated temperatures is larger in the tail part sample, where the recombination rate is dominated by recombination processes in the bulk wafer, as explained later.

We determined J_0 using the Kane-Swanson method (Fig. 3/e. and Fig. 4/e.), applying Auger lifetime corrections using the most recent temperature independent Auger lifetime model [6]. The exponential increase is governed by the temperature dependency of $n_i(T)$. However, it is worth investigating the slope of the Kane-Swanson plot (Eq.4.) itself, since in this case the n_i^2 factor which is included in any J_0 formulas is compensated, and therefore reflects the temperature dependence of the surface recombination processes, the diffusion length and diffusivity of charge carriers in the emitter layer, which is proven to be significant (Fig. 3/f. and Fig.

4/f.). The slope of the K-S plot decreases up to 50 °C, which indicates that the surface recombination characteristics are also improved. Over this temperature, we observe a slight increase of the slope. The origin of this has not been clarified yet. We found that the neglected temperature dependence of the Auger recombination cannot influence the results significantly. Previous temperature-dependent model predicts 10% change in the intrinsic lifetime in the investigated temperature range [7], however, carrier lifetime results are one order of magnitude lower than the Auger-limit, which reduces the relative error down to 1%. A possible reason can be the inaccuracy of the applied Klassen's carrier mobility model in this high temperature and injection level range, so it requires further investigation. These outlying data points do not limit us to draw general conclusions, as MPP lies at lower Δn regime.

We put the most important lifetime and efficiency data in a table. We present the bulk lifetime (τ_{bulk}) according to previous measurements on the same ingot before slicing. We observed different lifetime values at $\Delta n=10^{15}$ cm^{-3}, which indicates that the cell processing (phosphorous gettering, surface passivation) determines the recombination properties. On the tail-part sample the lifetime is significantly lower due to the segregated metal contaminants, which implies that the surface recombination is negligible in this case. The lifetime increases with the temperature by roughly 30% at 60°C for each sample. We observed increasing Kane-Swanson slope at the top and middle-part samples, which indicates improving surface passivation. Overall, the recombination lifetime is increasing for each sample independently from the contamination level. This results in a slightly improved temperature coefficient, ignoring the reducing effect of $n_i(T)$.

Table 1. *The most important lifetime and efficiency data from the top, middle and tail part wafers.*

	Top	Middle	Tail
$\tau(\Delta n=10^{15}$ cm^{-3}, T=30 °C)	315.4 µs	164.8 µs	38.21 µs
$\tau_{bulk}(\Delta n=10^{15}$ cm^{-3})	279.1 µs	367.5 µs	16.94 µs
Max. implied η (30-60 °C)	23.08 - 20.5 %	23.48 - 21 %	21.8 - 19.2 %
$\tau_{maxPP}(\Delta n=10^{15}$ cm^{-3}, T=30 °C)	263 µs	145 µs	26 µs
Δn(max. PP)	$1.4\cdot10^{14}$ cm^{-3}	$1.1\cdot10^{14}$ cm^{-3}	$2\cdot10^{13}$ cm^{-3}
Relative temperature coefficient	-0.356 rel%/°C	-0.349 rel%/°C	-0.375 rel%/°C

4. Conclusions

We realized a PCD measurement setup with alternating probing and light induced heating cycle. Stable elevated temperature can be reached between 30 °C and 60 °C. The main driving force behind the temperature dependency of implied η(T) and J_0(T) is $n_i(T)$ which has exponential temperature dependency. Our measurements show that both the bulk and surface recombination processes improved at higher temperatures. So, $\tau(\Delta n)$ increases at elevated temperatures resulting in a slight increase of the implied η(T) and reduction of J_0(T) respectively to the $n_i(T)$ changes. The $\tau(\Delta n$,T) affects the temperature coefficient of the cells positively. This phenomenon was observed in all samples regardless of the seriousness of metal contamination.

Data availability statement

Data supporting this study are only available on request due to our company policy. Please contact gergely.havasi@semilab.hu

Author contributions

Gergely Havasi: Formal Analysis, Investigation, Project administration, Visualization, Writing – original draft, **Dávid Krisztián**: Methodology, Supervision, Validation, Writing – review & editing, **Ferenc Korsós**: Conceptualization. Supervision, Validation, Writing – review & editing, **Shaoyong Fu**: Resources

Competing interests

The authors declare that they have no competing interests.

References

[1] R. A. Sinton, A. Cuevas and M. Stuckings, “Quasi-steady-state photoconductance, a new method for solar cell material and device characterization”, Conference Record of the Twenty Fifth IEEE Photovoltaic Specialists Conference - 1996, Washington, DC, USA, 1996, pp. 457-460, doi: 10.1109/PVSC.1996.564042.

[2] M. J. Kerr, A. Cuevas, R. A. Sinton, “Generalized analysis of quasi-steady-state and transient decay open circuit voltage measurements” Journal of Applied Physics 91, 399 (2002)

[3] D. E. Kane, R. M. Swanson, “Measurement of the emitter saturation current by a contactless photoconductivity decay method”, Stanford Electronics Laboratories, McCullough 204 Stanford, 1985

[4] D.B.M. Klaassen, A unified mobility model for device simulation—II.Temperature dependence of carrier mobility and lifetime. Solid-State El-ectronics, Volume 35, Issue 7, 1992, Pages 961-967, https://doi.org/10.1016/0038-1101(92)90326-8.

[5] M. A. Green, “Intrinsic concentration, effective densities of states, and effective mass in silicon” J. Appl. Phys. 67, 2944 (1990); doi: 10.1063/1.345414

[6] T. Niewelt, B. Steinhauser, A. Richter, B. Veith-Wolf, A. Fell, B. Hammann, N. E. Grant, L. Black, J. Tan, A. Youssef, J. D. Murphy, J. Schmidt, M. C. Schubert, S. W. Glunz, “Reassessment of the intrinsic bulk recombination in crystalline silicon”, Solar Energy Materials and Solar Cells, 235 (2022), 111467. https://doi.org/10.1016/j.solmat.2021.111467

[7] P. P. Altermatt, J. Schmidt, G. Heiser, A. G. Aberle, Assessment and parameterization of Coulomb-enhanced Auger recombination coefficients in lowly injected crystalline silicon. Journal of Applied Physics 82, 4938 (1997); doi:10.1063/1.366360